Available online at www.sciencedirect.com
ScienceDirect
Applied Surface Science 253 (2007) 6672–6680
applied surface science
www.elsevier.com/locate/apsusc

Fundamentals and applications of ion–ion plasmas

Demetre J. Economou *

Plasma Processing Laboratory, Department of Chemical and Biomolecular Engineering, University of Houston, Houston, TX 77204-4004, USA

Available online 4 February 2007

Abstract

Ion–ion plasmas can form in the late afterglow of pulsed discharges or downstream of continuous wave discharges in electronegative gases. In ion–ion plasmas, negative ions replace electrons as the negative charge carriers. In the absence of electrons, ion–ion plasmas behave quite differently compared to conventional electron–ion plasmas. Application of a radio frequency bias to a substrate immersed in an ion–ion plasma can be used to extract alternately positive and negative ions, thereby minimizing charging on device features during micro-device fabrication. Ion–ion plasmas are also important in negative ion sources, dusty plasmas, and the D-layer of the earth's atmosphere.

Keywords: Pulsed plasma; Afterglow; Charging damage; Negative ions; Simulation

1. Introduction

Electronegative gas plasmas are widely used in microelectronics manufacturing for etching and deposition of thin films [1,2]. For example, plasmas in gases containing Cl_2 or SF_6 are used for silicon etching, fluorocarbon plasmas are indispensable for silicon dioxide etching, and oxygen plasmas are used for ashing of photoresist and other polymers. Electronegative plasmas often consist of a core where the negative ions accumulate, followed by a zone devoid of negative ions, followed by a positive ion sheath near the wall. At high negative ion concentration, the electronegative core expands all the way to the sheath edge. This ''stratification'' of electronegative plasmas has been studied extensively, especially for collisional plasmas [2–5]. The structure of the potential in the plasma including abrupt transitions or oscillations has also been reported [6–8]. In continuous wave plasmas, the electrostatic fields are strong enough to trap negative ions in the plasma. Thus the negative ion flux to the wall is essentially zero. This is not the case for pulsed plasmas, however.

Pulsed plasma operation (in which the plasma power is modulated with a given repetition frequency and duty cycle) can apparently ameliorate anomalous etch profiles (e.g., notching) and other undesirable effects that occur in conventional continuous wave discharges. In a continuous wave discharge, positive ions bombarding the wafer have a strongly anisotropic velocity distribution, while electrons have an almost isotropic velocity distribution (Fig. 1). As a result, positive ions can penetrate deeply into a trench charging the trench bottom positively, while electrons deposit their charge on the sidewalls of the trench. Such differential charging, and associated etch profile distortions, are thought to be a major problem for the fabrication of the next generation of microdevices. The divergence of oncoming ions due to differential charging of microstructures on the wafer surface may also cause reduction of the ion flux as a function of depth in the micro-feature, leading to aspect ratio dependent etching (ARDE), or even etch stop [9].

The situation becomes more favorable in pulsed-power discharges. Studies indicate that extraction of charged species from the afterglow plasma and their acceleration towards a radio frequency (RF) biased electrode could reduce charging damage and improve etching characteristics [10–12]. For instance, greatly improved etch performance has been reported in pulsed-power chlorine discharges by applying a low frequency bias to the substrate in the afterglow of an inductively coupled plasma source. It was suggested that low frequency bias results in alternate acceleration of positive and negative ions extracted out of the plasma. Since positive and negative ions have almost equal masses and similar velocity anisotropy under the influence of RF bias, the net charge deposited on the wafer surface should be greatly reduced, ameliorating charge-induced damage.

* Tel.: +1 713 743 4320; fax: +1 713 743 4323.
E-mail address: economou@uh.edu.

0169-4332/$ – see front matter © 2007 Elsevier B.V. All rights reserved.
doi:10.1016/j.apsusc.2007.02.004

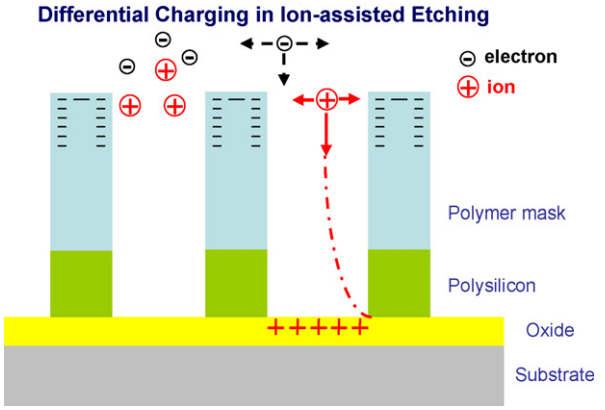

Fig. 1. Differential charging of micro-features on a wafer during conventional electron–ion plasma processing. Charging can deflect oncoming ions to strike the sidewalls and create damage.

Ion–ion plasmas are plasmas in which the negative charges are negative ions instead of electrons. In practice, some electrons may still be present. Ion–ion plasmas may form in the (temporal) afterglow of pulsed discharges in electronegative gases [13,14]. The plasma grows during power ON (active-glow) and decays during power OFF (afterglow). For a long enough afterglow, the electron concentration in the plasma diminishes to the point that negative ions become the dominant negative charge carrier, forming an ion–ion plasma. One can also have a spatial afterglow in a flowing plasma, sustained by a continuous wave power source. Far enough downstream of the plasma generation zone, the electron concentration can decay substantially to form an ion–ion plasma. For the plasmas of interest, electron decay is mainly by electron attachment to electronegative gases (e.g., chlorine, sulfur hexafluoride and oxygen) and diffusion to the walls of the reactor.

Ion–ion plasmas find application in charge-free semiconductor manufacturing [10–12,15], negative ion sources [16,17], and the D-layer of the upper atmosphere [18]. Some dusty plasmas can also be considered as ion–ion plasmas since dust particles "soak" electrons to form massive "negative ions". Samukawa et al. presented a fast neutral beam source based on formation of an ion–ion plasma [15]. The ion–ion plasma was formed in the afterglow of a pulsed inductively coupled discharge in an electronegative gas (Cl_2 or SF_6). A positive bias voltage was applied to the extraction electrode during the afterglow attracting negative ions. The extraction electrode had high aspect ratio through holes. Negative ions suffered grazing angle collisions with the internal surfaces of the holes turning into fast neutrals. Charge exchange with neutral gas may also play a role at higher pressures. The concept of neutral beam generation by ion extraction and neutralization through a grid was implemented in an earlier design by Panda et al. [19]. A common negative ion source is that in hydrogen gas for the production of negative H^- ions [16,17]. These ions are eventually accelerated and neutralized before being injected in fusion reactors to assist in heating. To produce H^-, a pulsed plasma in hydrogen gas is used. Highly excited vibrational states of molecular hydrogen formed in the active glow attach cold electrons in the afterglow to form negative ions. These ions are extracted by application of a bias through an aperture at the reactor wall. The presence of a weak magnetic field can modify the structure of the potential field close to the extraction hole of the negative ion source, thereby enhancing the extracted negative ion flux [20]. An electron-free fullerene ion–ion plasma was recently generated with equal mass of positive and negative ions [21]. The basic characteristics of this plasma were discussed including the absence of a sheath.

2. Characteristics of ion–ion plasmas

Much of the conventional thinking applied to traditional plasmas containing electrons is not applicable to ion–ion plasmas. For example, in ion–ion plasmas, the plasma potential does not have to be the most positive potential in the system (as in electron–ion plasmas). In fact, the potential profile across an ion–ion plasma can be monotonically decreasing from one electrode to the other [22], much like in liquid electrolytes [23].

The electrostatic fields in an ion–ion plasma are determined by negative ions instead of electrons. In conventional electron–ion plasmas, electrostatic fields form naturally to balance the losses of the lighter and more energetic electrons from the plasma, with the losses of the heavier and colder positive ions. By replacing electrons with negative ions in the plasma, the mass and the energy of the negatively and positively charged species become comparable. Ion–ion plasmas, therefore, are characterized by significantly weaker electrostatic fields with a plasma potential determined by the ion temperature (in conventional plasmas it is determined by the electron temperature). In the limiting case of both positive and negative ions having equal mass (e.g., Cl^+ and Cl^-) and temperature, ion–ion plasmas are characterized by the absence of electrostatic fields, zero plasma potential, and no sheaths (with no bias voltage applied). In such case, the spatial profiles of positive and negative ions coincide throughout the reactor and both species are able to diffuse freely to the walls.

The Debye length λ_D in the presence of negative ions can be expressed as

$$\frac{1}{\lambda_D} = \sqrt{\left(\frac{\alpha}{kT_n} + \frac{1-\alpha}{kT_e}\right)\frac{e^2 p}{\varepsilon_0}} \quad (1)$$

where $\alpha = n/p$ is the ratio of negative ion to positive ion density, and T_n, T_e are the negative ion and electron temperature, respectively. For an ion–ion plasma, $\alpha = 1$, and the Debye length $\lambda_{D,ii}$ becomes,

$$\lambda_{D,ii} = \sqrt{\frac{\varepsilon_0 kT_n}{e^2 p}} \quad (2)$$

The Debye length in an ion–ion plasma is clearly determined by the ion temperature. Features of ion–ion plasmas include [24]: (a) vanishingly small space charge fields (see Eq. (5) below), (b) both positive ions and negative ions can be readily extracted from the plasma (see Fig. 3 below), (c) only heavy particle reactions dictate the plasma chemistry, (d) the plasma impedance can be changed drastically by irradiating the plasma

with light of appropriate wavelength as to detach negative ions (plasma behaves as an on-off switch), and (e) a single Langmuir probe will give an almost symmetric *I–V* characteristic in an ion–ion plasma [25,26].

3. Formation of ion–ion plasmas

Ion–ion plasmas may be formed in the afterglow of pulsed discharges in electronegative gases [27,28]. They may also form downstream of continuous wave discharges in strongly electronegative gases (spatial afterglow). Fig. 2 shows the evolution of species densities and electron temperature at the center of a parallel plate pulsed chlorine discharge (20 mtorr, 1 W/cm^3 power density, no applied electrode bias), once a periodic steady-state is achieved [13]. The time window 0–50 μs represents the time power is "ON" (activeglow) while the time window 50–100 μs represents the time power is "OFF" (afterglow) during a pulse. For convenience, the overall evolution during a pulse is divided into four different regimes (see Fig. 3): (I) early activeglow, (II) late activeglow, (III) early afterglow and (IV) late afterglow. The overall trends shown in Fig. 2 are in agreement with experimental results reported in the literature [12,29–31]. The electron temperature shows the formation of a sharp spike as soon as the power is switched "ON", levels out in the late activeglow, and then drops abruptly in the early afterglow. The electron density shows a large variation of several orders of magnitude between the activeglow and the afterglow, while the negative ions are considerably less modulated. The peak in negative ion density forming immediately after the plasma power is turned OFF (at 50 μs), is due to rapid attachment of cool electrons to chlorine molecules. The plasma is weakly electronegative in the activeglow and then becomes increasingly more electronegative in the afterglow.

Electrons are lost rapidly in the early afterglow by ambipolar diffusion to the walls and dissociative attachment while negative

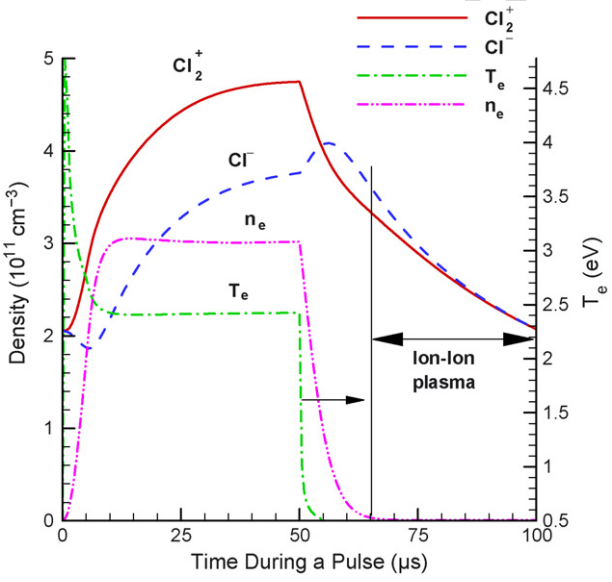

Fig. 2. Calculated time variation of species densities and electron temperature in a high density pulsed plasma through chlorine. Power density 1.0 W/cm^3, pressure 20 mtorr, pulse period 100 μs, and duty cycle 50%. From Ref. [13].

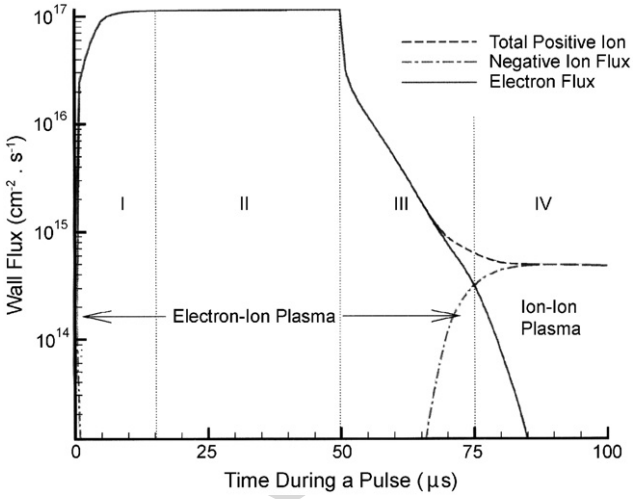

Fig. 3. Calculated time variation of species fluxes striking an unbiased electrode in a high density pulsed plasma through chlorine. Power density 1.0 W/cm^3, pressure 20 mtorr, pulse period 100 μs, and duty cycle 50%. From Ref. [13].

ions are still trapped in the reactor. Once the electron density becomes low enough (see below), negative ions become the dominant negative charge carrier in the plasma. The electric field is now determined by negative ions instead of electrons and there is an abrupt transition from an electron-dominated plasma to an ion–ion plasma. Negative ions can now exit the plasma (Fig. 3). The ion–ion plasma is characterized by weak electrostatic fields (Eq. (5) below) and a diffusive flux of negative ions to the walls. After the transition to an ion–ion plasma, electrons are no longer confined in the plasma and are lost at a faster rate which eventually approaches the limit of free diffusion of electrons to the walls in the (near) absence of electrostatic fields. The positive and negative ion densities decay together much more slowly due to ion–ion recombination and diffusion losses to the walls.

In a collisional electronegative plasma containing electrons, one kind of positive ions and one kind of negative ions, the electrostatic field in the bulk is given by [13]

$$E = \frac{D_p \nabla p - D_n \nabla n - D_e \nabla n_e}{b_p p + b_n n + b_e n_e} \tag{3}$$

here p, n, and n_e are the positive ion, negative ion and electron density, respectively, and D_p, D_n and D_e, and b_p, b_n and b_e are the diffusivities and mobilities of these species, respectively. When $n/n_e \ll b_e/(b_n + b_p)$, the plasma is electron dominated and the electric field becomes

$$E = -\frac{T_e}{e}\frac{\mathrm{d}\ln n_e}{\mathrm{d}x} \tag{4}$$

where T_e is the electron temperature. This is the familiar expression for conventional electron–ion plasmas.

The condition $n/n_e = b_e/(b_n + b_p)$, signifies a transition to an ion–ion plasma, and when $n/n_e \gg b_e/(b_n + b_p)$, the ion–ion plasma is fully formed. In the ion–ion plasma, the electrostatic field is

$$E = \frac{(D_p - D_n)\nabla n}{(b_p + b_n)n} \tag{5}$$

Eq. (5) shows that the electrostatic fields in an ion–ion plasma are indeed weak since the positive and negative ion diffusivities are generally comparable. If $D_p = D_n$ (e.g., equal ion masses and temperatures), the electric field is identically zero. In such case, positive and negative ions are diffusing freely.

The decay of electronegative plasmas in the afterglow of pulse discharges under a variety of situations has been studied by Kaganovich et al. [32]. The time needed for negative ions to reach the wall is of importance for applications based on negative ion extraction. For a three-component plasma (electrons, negative ions and positive ions), where all three species have the same temperature T_i, this time is given by

$$t_{n,out} = \frac{(2L)^2}{2\pi^2 b_i T_i}\left(\frac{p_0}{n_0}\right) \quad (6)$$

where L is the plate separation, b_i the ion mobility, and p_0, n_0 are the positive and negative ion density, respectively, at the beginning of the afterglow. This has practical significance, despite the assumption of equal temperatures, since the electron temperature normally plummets within a few microseconds in the afterglow to very low values. Eq. (6) indicates that the time it takes for the negative ions to reach the wall is shorter for higher electronegativities (as electronegativity increases, n_0 approaches p_0).

In Fig. 3, the transition from an electron–ion plasma to an ion–ion plasma is characterized by the electron flux becoming equal to the negative ion flux at the walls ($t = 75$ μs). The positive ion flux, which initially overlaps with the electron flux in the early afterglow becomes equal to the negative ion flux in the late afterglow. Experimental results reported by Smith et al. [33] in the afterglow of an oxygen plasma show similar behavior. The negative ion flux was negligible in the early afterglow and abruptly increased by several orders of magnitude to become equal to the positive ion flux in the late afterglow.

A schematic of a spatial afterglow for the possible production of an ion–ion plasma is shown in Fig. 4. The continuous wave (no pulsing) electronegative plasma is produced by an inductive "stove-top" antenna coil powered with a radio frequency source. As the plasma diffuses downstream, electrons attach to negative ions and diffuse to the walls. Far enough downstream the electron density diminishes to the point that an ion–ion plasma may form over the wafer. A magnetic filter to spatially separate electrons from ions can help, but in practice some residual electrons may still persist. Gas flow brings fresh reactants to the wafer surface. A bias voltage applied to the substrate electrode can extract and accelerate positive and negative ions to effect etching of the wafer. Since the mass and velocity anisotropy of the positive ions are similar to those of negative ions, differential charging of micro-features on the wafer surface (Fig. 1) may be reduced.

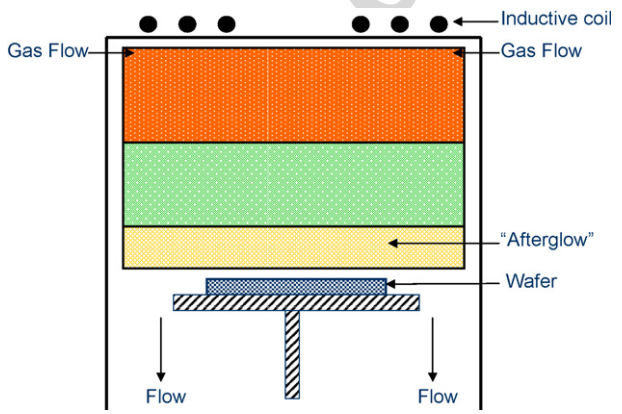

Fig. 4. Spatial afterglow formed downstream of a continuous wave (no pulsing) plasma. A radio frequency bias can be applied to the substrate electrode to accelerate negative and positive ions to the surface.

4. RF biasing of an ion–ion plasma

Consider an ion–ion plasma with equal positive and negative ion masses (e.g., Cl^+ and Cl^-) and temperatures. Without applied bias, the positive-ion density simply overlaps with the negative-ion density, and there is no sheath formed near the electrodes. In the presence of a bias potential, however, the positive and negative ions separate to form ion–ion sheaths near the electrode. A one-dimensional fluid model of an ion–ion plasma (with no residual electrons) was developed which resolved the sheath regions near the walls. The model included the Poisson equation for the electrostatic field coupled with the continuity and momentum equations of the ion density and velocity [22].

Some important results of the simulation are summarized as follows: (a) Due to the equal masses and temperatures of the positively and negatively charged species in the ion–ion plasma, the applied bias is distributed symmetrically between the electrodes. No DC bias potential is formed between the electrodes. (b) Each electrode reverses polarity with respect to the bulk plasma during a bias period. Consequently, the net charge in the ion sheath next to the electrode also changes polarity, with a net negative charge existing in the sheath for an equal duration as a net positive charge. This is in contrast to electron–ion plasmas in which the sheath has a net positive charge. (c) Due to the lower temperature and greater mass of negative ions compared to electrons, the sheath structure in ion–ion plasmas changes significantly as the bias frequency is varied. For low bias frequencies (100 kHz), the charge distribution is monotonic during each half cycle. For intermediate frequencies (10 MHz), when the bias period approaches the ion transit time through the sheath, double layers form with both positive and negative charges coexisting in the sheath. For high frequencies (e.g., 60 MHz), beyond the ion plasma frequency, plasma waves are launched from the bulk plasma, and the sheath consists of multiple peaks of positive and negative charge (multiple double layers).

Results shown below are for a one-dimensional ion–ion plasma (Cl^+ and Cl^- and no electrons) at 20 mtorr, 3.8 cm electrode gap, and 130 V peak-to-peak applied bias. The sinusoidal bias was applied to the left electrode, such that the electrode had a negative potential during the first half of the cycle ($0 < \tau < 0.5$) and a positive potential during the second

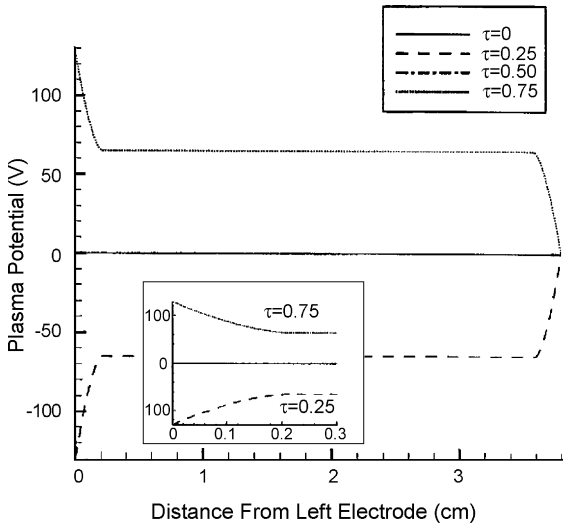

Fig. 5. Calculated potential distribution in an ion–ion plasma when a 100 kHz bias voltage (130 V peak-to-peak) is applied to the electrode at $x = 0$. From Ref. [22]. An expanded scale is shown in the insert.

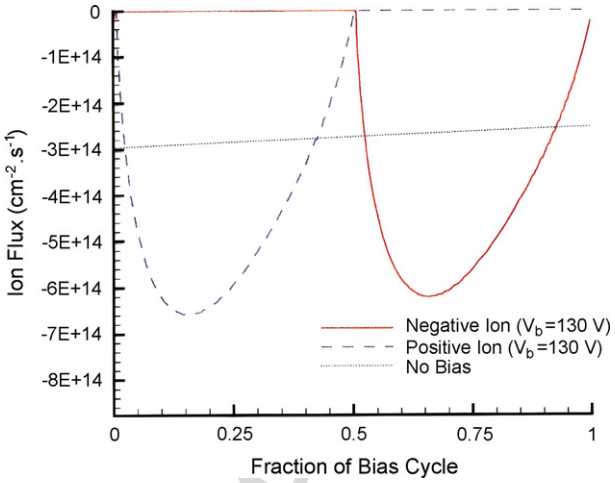

Fig. 6. Calculated time evolution of the negative ion and positive ion flux bombarding an electrode in contact with an ion–ion plasma under the influence of a 100 kHz bias (130 V peak-to-peak). The dashed line shows the diffusion flux in the absence of bias. From Ref. [22].

half of the cycle ($0.5 < \tau < 1$). The right electrode was kept at zero potential at all times. The peak ion density at the plasma center was 10^{11} cm^{-3}.

The potential distribution across the electrode gap for four times during the RF cycle is shown in Fig. 5, for an applied frequency of 100 kHz. In contrast to conventional electron–ion plasmas, the plasma potential is not the most positive potential in the system. In fact, the potential distribution is monotonic much like in liquid electrolytes [23]. The applied frequency is low enough (much lower than the ion plasma frequency) for the potential to be ''shielded'' out of the bulk plasma. The potential drop in the bulk is negligible, with most of the potential dropped across the sheaths. When the electrode potential is positive with respect to the bulk, the sheath adjacent to that electrode has a negative charge. When the electrode potential is negative with respect to the bulk, the sheath adjacent to that electrode has a positive charge. This is also in contrast to conventional plasmas for which the electrode sheath has (almost) always a net positive charge.

Fig. 6 shows the evolution of ion fluxes at the left (biased) electrode during a RF cycle for a bias frequency of 100 kHz. For this low operating frequency, the left electrode is bombarded alternately by positive ions (dashed line) and negative ions (solid line) during each half of the RF cycle. The peak in the negative ion flux is slightly less than the peak in the positive ion flux due to continuous depletion of the plasma. At this relatively low operating frequency, a significant fraction of the plasma is depleted during the course of each half cycle. Depletion of ions is also seen even without applied bias. At any instant of the cycle, the flux of positive ions exiting the plasma at one electrode is equal to the flux of negative ions exiting the other electrode (not shown). Fig. 6 also shows that the peak ion flux during a half cycle is comparable to twice the diffusion flux of ions without a bias (dotted line). The total ion flux integrated over a full cycle is equivalent to the diffusion flux of ions without a bias. Therefore, for low bias frequencies, the flux of ions bombarding the electrode is independent of magnitude of the applied bias and is limited by the ion diffusion flux. The only effect of the applied bias is to temporally redistribute this diffusion flux between the two electrodes. Instead of exiting both electrodes simultaneously, the positive ions exit only the negatively biased electrode while the negative ions exit only the positively biased electrode during each half cycle. The RF bias, however, increases the ion energy.

Fig. 7 shows the evolution of the ion fluxes at the left electrode during the course of a RF cycle for a bias frequency of 10 MHz, which is close to the ion plasma frequency evaluated at the sheath edge. The effects of the transit time of ions through the sheath are clearly evident in the evolution of fluxes. The positive ion flux continues till $\tau = 0.7$ even when the electrode is positively biased with respect to the plasma. Negative ion flux does not appear till $\tau = 0.8$ representing the transit time of the

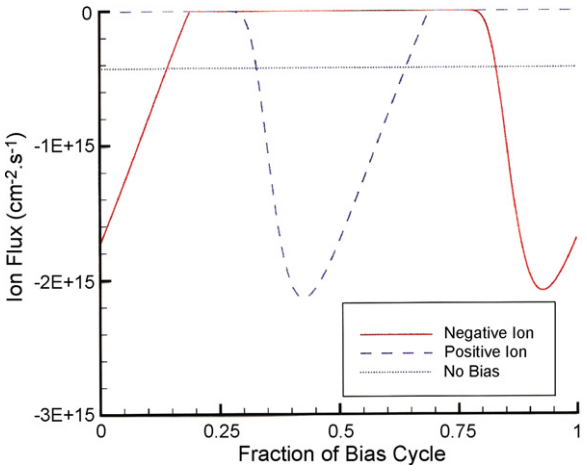

Fig. 7. Calculated time evolution of the negative ion and positive ion flux bombarding an electrode in contact with an ion–ion plasma under the influence of a 10 MHz bias (130 V peak-to-peak). The dashed line shows the diffusion flux in the absence of bias. From Ref. [22].

negative ion front through the sheath. In contrast to the low frequency case, the ion flux is significantly greater than the corresponding diffusion flux (dotted line) without an applied bias. At this bias frequency, there is insufficient time for the applied bias to be fully shielded in the sheath regions. Due to the presence of relatively high electric fields in the bulk plasma, the ion flux to the walls exceeds the diffusion flux. Consequently, a relatively high bias frequency, approaching the (ion) plasma frequency is required to extract ions at a faster rate from the plasma.

Fig. 8 shows the evolution of the ion flux at the left electrode during a RF cycle for a bias frequency of 60 MHz. Since the ions are no longer able to respond to the applied frequency, the perturbation in the ion velocities due to the applied bias is small. The ion fluxes, therefore, are only weakly modulated by the applied bias. The electrode is now continuously bombarded by both positive and negative ions throughout the cycle with an average flux equal to the diffusion flux of the ions. As a result of a net displacement toward the electrode, a peak in the negative ion flux is formed at $\tau = 0.5$ while a peak in the positive ion flux is formed at $\tau = 1.0$.

Based on the ion flux evolution at the electrode, operation in the intermediate frequency regime appears advantageous for rapidly extracting ions form the plasma at the conditions examined (20 mtorr pressure and bias potential of 130 V). At low frequencies (e.g., 100 kHz), alternate bombardment by the positive ions and negative ions is possible but the ion flux is limited by the diffusion flux in the bulk plasma. Alternate bombardment of the electrode by positive and negative ions is also possible with intermediate values of frequency (e.g., 10 MHz), albeit with a finite phase lag with respect to the applied bias. There is less time for collisional drag to limit the ion flux at intermediate frequencies, and ions may be extracted at a faster rate from a plasma compared to low frequencies. Increasing the bias frequency (e.g., 60 MHz) beyond the ion plasma frequency, results in trapping the ions in the plasma and the ion flux at the electrode is essentially reduced to the diffusion flux of the ions.

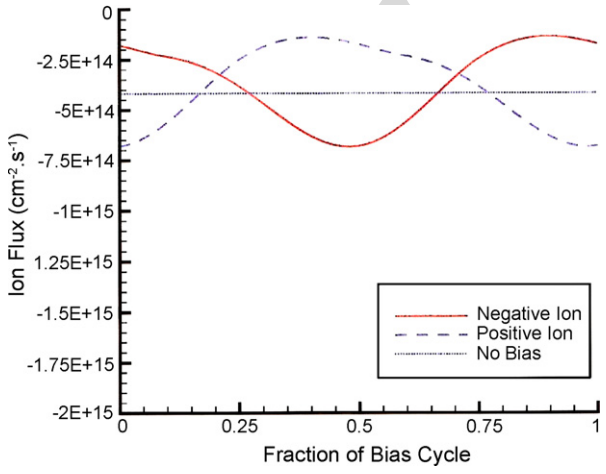

Fig. 8. Calculated time evolution of the negative ion and positive ion flux bombarding an electrode in contact with an ion–ion plasma under the influence of a 60 MHz bias (130 V peak-to-peak). The dashed line shows the diffusion flux in the absence of bias. From Ref. [22].

Alternate extraction of positive and negative ions from an ion–ion plasma is shown in Fig. 9 [34]. A 1 mtorr chlorine plasma was generated with 13.56 MHz power having a pulse repetition frequency of 1 kHz and a duty cycle of 50%. This corresponds to activeglow (power ON) and afterglow (power OFF) periods of 500 μs each. The applied power was 300 W during the activeglow. Ten cycles of a sinusoidal bias voltage (225 V peak) filled the 500 μs of the afterglow period. This bias was applied to the substrate electrode and was turned off during the activeglow. The substrate electrode had a 100 μm diameter pinhole for sampling ions that were detected by a differentially pumped mass spectrometer behind the electrode. The goal was to create an ion–ion plasma during the afterglow, and extract negative ions to the substrate by the application of substrate bias during that afterglow. The left half of Fig. 9 corresponds to the activeglow (0–500 μs) and the right half to the afterglow (500–1000 μs).

Fig. 9(a) shows the Cl_2^+ and Cl^- signals. The Cl_2^+ signal is delayed by $\Delta t_{TOF} = 50$ μs corresponding to the time of flight through the mass spectrometer. The Cl_2^+ signal increases

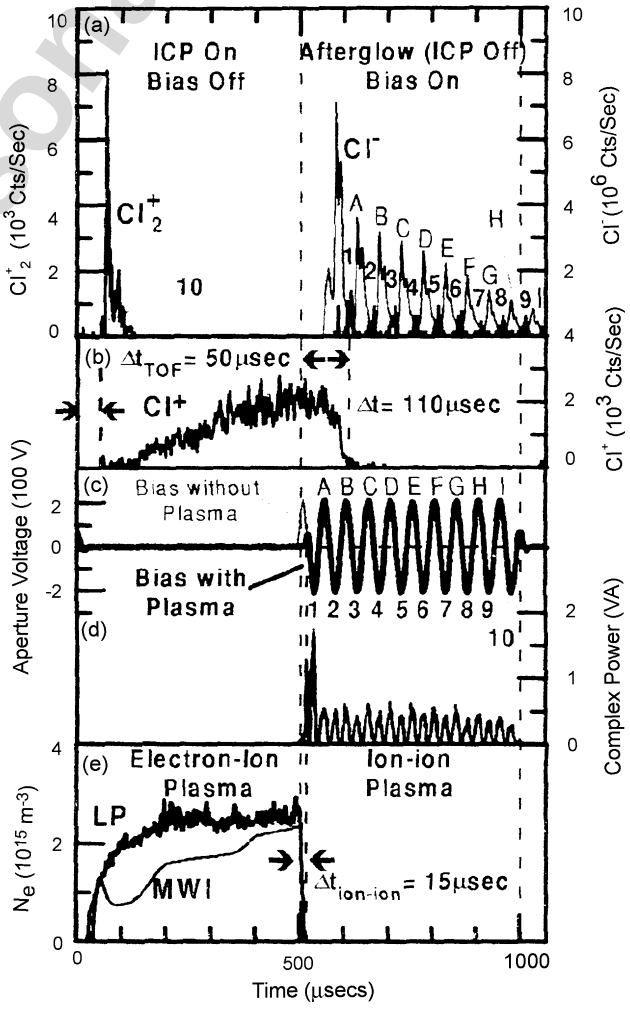

Fig. 9. Measurement of chlorine positive ions and negative ions bombarding a substrate in contact with an ion–ion plasma under the influence of bias. The (volumetric) electron density is shown in (e). The plasma source was pulsed ON (0–500 μs) and OFF (500–1000 μs). During plasma OFF (afterglow) a 100 kHz bias was applied to the substrate. See text for more details. From Ref. [34].

rapidly as power is turned on in the activeglow, but quickly decays to small values. At the same time, the Cl^+ signal increases (Fig. 9(b)) in the activeglow, only to decay early in the afterglow as Cl^+ is converted to Cl_2^+ by charge exchange. In the afterglow, one observes Cl^- peaks (designated by letters A, B, C, . . ., I) alternating with Cl_2^+ peaks (designated by numbers 1, 2, 3, . . ., 9) as shown in Fig. 9(a). The Cl^- peaks correspond to the positive peaks of the bias voltage, while the Cl_2^+ peaks correspond to the negative peaks of the bias voltage (Fig. 9(c)). The peak value of the ion signal decays (Fig. 9(a)) as the ion–ion plasma is depleted by extraction and recombination in the afterglow. (The relative peak heights are not important here because the sensitivity of the mass spectrometer to these positive and negative ions was not measured.) This experiment demonstrated alternate irradiation of the substrate by positive ions and negative ions. The fact that an ion–ion plasma forms in the afterglow is corroborated by the electron density traces of Fig. 9(e). Both Langmuir probe and microwave interferometry indicate that the electron density increases during the activeglow and decays to negligible values after $\Delta t_{ion-ion} \sim 15$ μs into the afterglow. It is the electron decay and formation of an ion–ion plasma that allows negative ions to escape. Evidently the bias applied in the afterglow is not high enough to heat the remaining electrons and re-establish a potential well deep enough to trap the negative ions [14,30].

The injection of negative charges by the application of a bias to the substrate electrode in a power modulated dual-frequency capacitively coupled plasma was demonstrated in Ref. [35]. A schematic of the system is shown in Fig. 10(a). Plasma

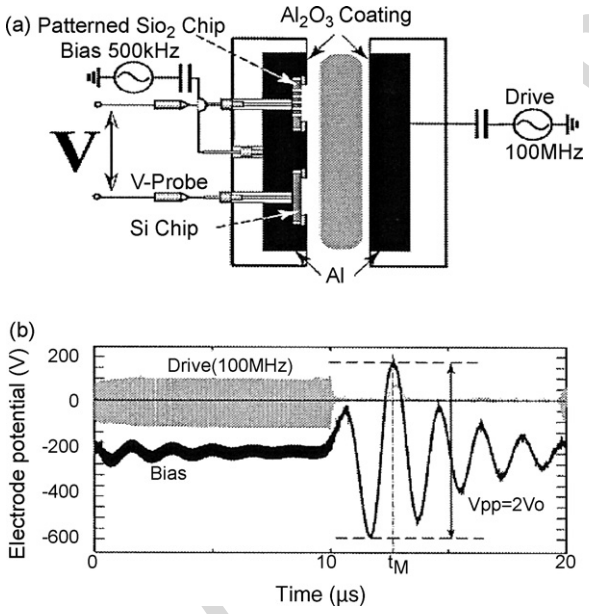

Fig. 10. (a) Schematic of a dual frequency capacitively coupled reactor. Plasma drive power (at 100 MHz) was pulsed repetitively ON for 10 μs and OFF also for 10 μs. A bias voltage was applied to the substrate electrode having a patterned (with submicron holes) silicon dioxide chip and a silicon reference chip. The voltage difference between these chips is an indication of the degree of charging of the bottom of the holes in silicon dioxide. (b) Potential vs. time for the 100 MHz drive and the substrate bias. The substrate bias swings positive for a short time in the afterglow (at time t_M). The peak-to-peak voltage at time t_M is $2V_0$. From Ref. [35].

was generated by a 100 MHz power modulated 10 μs ON (activeglow) and 10 μs OFF (afterglow). The peak voltage during power ON was 110 V (25 W) in a 25 mtorr CF_4/Ar (10–90% by volume) gas mixture. The substrate was equipped with two test chips: (a) a patterned chip having 0.5 μm diameter, 2.5 μm deep holes in SiO_2 on silicon (10% open area) isolated electrically from the substrate electrode, and (b) an equal size un-patterned silicon chip. The voltage difference between the bottoms of the patterned oxide chip and the un-patterned silicon chip was a measure of charging of the hole bottoms (referred to as bottom charging voltage below). The electrode potentials during a complete power pulse are shown in Fig. 10(b). The 100 MHz "drive" power is ON for 10 μs and OFF for the remaining 10 μs. The bias voltage is negative during power ON but swings temporarily positive (peak-to-peak value $2V_0$) at time t_M during the afterglow.

The bottom charging voltage is shown in Fig. 11 for the CF_4/Ar (left) and pure argon (right) plasmas. Curves labeled (II) correspond to a value of $t_M = 12.5$ μs (2.5 μs into the afterglow) for different values of amplitude V_0 (see Fig. 10(b)). The bottom charging voltage is greatly reduced for high enough values of V_0. This is attributed to negative charge injection to the bottom of the holes of the patterned chip which partly neutralized the accumulated positive charge. This injection of negative charges is facilitated by electric field reversal (electric field pointing away from the substrate) during application of the positive bias which accelerated negative charge towards the substrate. There is no such neutralization observed in the argon plasma (Fig. 11(b)). Evidence for electric field reversal was also provided by a large enhancement of optical emission from the edge of the sheath over the substrate at exactly the time of the positive bias swing. Emission was monitored from argon atoms at 750.4 nm and argon ions at 434.8 nm, resulting from electronically excited species.

The curves labeled (I) in Fig. 11 show the bottom charging voltage when the positive swing of the applied substrate bias is made to occur 3 μs into the activeglow (not shown in Fig. 10(b)). The bottom charging voltage keeps on increasing implying that there is no injection of negative charges into the holes. Apparently, there is no electric field reversal occurring during the activeglow since the dominant negative charge carriers are electrons. The situation changes in the afterglow when negative ions are more plentiful compared to electrons and the electric field can apparently be reversed [36,37].

In their two-dimensional computational model of pulsed electronegative discharges, Subramonium and Kushner [14] found that the application of radio frequency substrate bias can lead to capacitive-mode (sheath) electron heating in the afterglow, which prevents extraction of negative ions. Electron heating does not allow the electron density and/or temperature to decay enough in the afterglow for an ion–ion plasma to form. High electronegativities and large bias voltages favored electron heating. On the other hand, high electronegativities are needed for a more rapid transition to an ion–ion plasma in the afterglow (see Eq. (6)). A mixed gas $Ar/Cl_2 = 40/60$ (by volume) plasma was found to best satisfy these competing requirements. They also found that pulsed (synchronous) bias

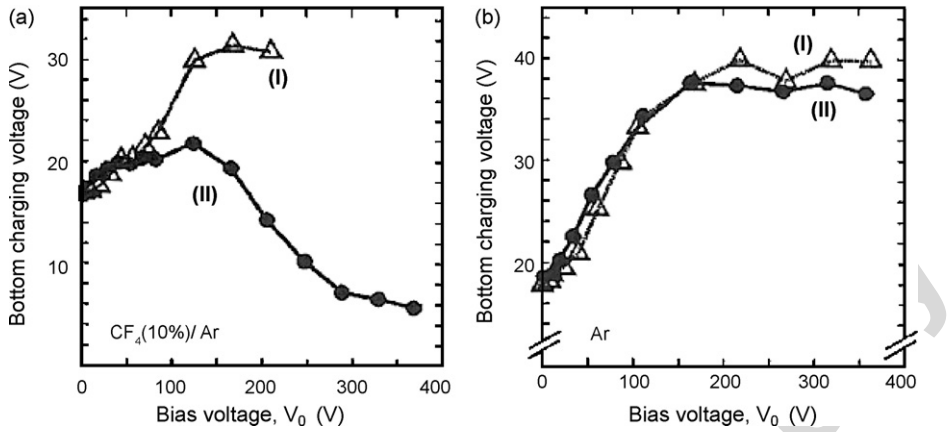

Fig. 11. Charging voltage of the bottom of the silicon dioxide holes as a function of V_0 for a CF_4 (10%)/Ar plasma (a), and an Ar plasma (b). Curves II correspond to the case where the bias voltage swing occurs at time t_M = 12.5 μs (2.5 μs into the afterglow) as shown in Fig. 10(b). Curves I correspond to the case where the bias voltage swing occurs at time t_M = 3 μs (into the activeglow) not shown in Fig. 10(b). From Ref. [35].

was more effective in extracting negative ions as compared to a continuous bias (still with pulsed plasma power).

Fig. 12(a) shows the extracted negative ion fluence during the last 50 μs of the afterglow as a function of bias voltage.

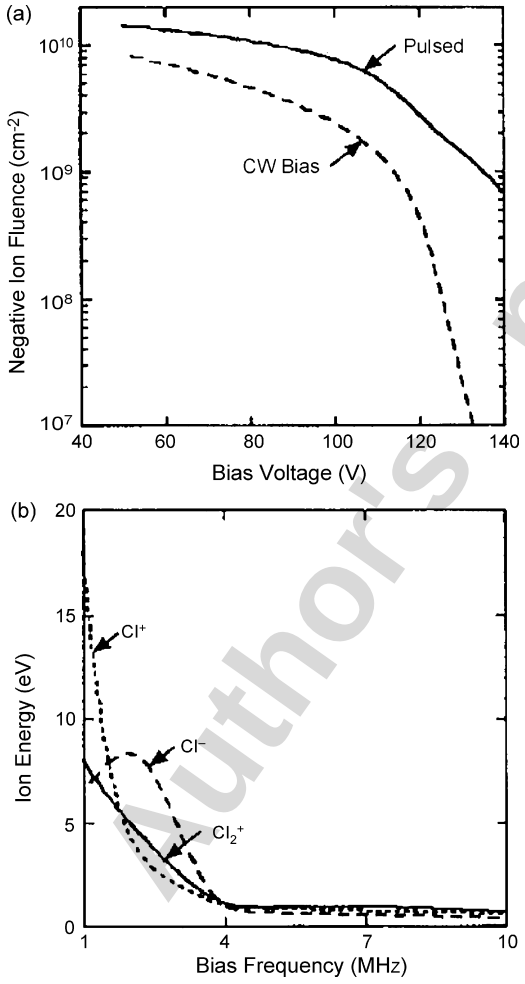

Fig. 12. (a) Negative ion fluence (during the last 50 μs of the afterglow) vs. bias voltage applied to the substrate electrode in a Ar (40%)/Cl_2 (60%) plasma, for continuous wave bias (dashed line) and pulsed bias (solid line). (b) Mean ion energy as a function of applied bias frequency for Cl_2^+, Cl^+ and Cl^-. See text for details. From Ref. [14].

Other conditions were: 10 mtorr of a Ar/Cl_2 = 40/60 plasma, total gas flow of 100 sccm, ICP peak power of 300 W at 10 MHz, modulated with a frequency of 6.67 kHz and a duty cycle of 33% (50 μs power ON, 100 μs power OFF), and a bias frequency of 10 MHz. Two kinds of bias voltages were applied. The cw bias was applied continuously, while the pulsed (synchronous) bias was applied for the last 50 μs of the 100 μs afterglow and the first 10 μs of the activeglow. The negative ion fluence is greatly enhanced with pulsed bias due to reduced capacitive heating. The difference is more dramatic at larger bias voltages, when cw bias can ''ignite'' a capacitive coupled plasma in the afterglow trapping negative ions. The average energy of the extracted ions (averaged over the last 50 μs of the afterglow), as a function of the pulsed bias frequency (for a bias voltage of 100 V), is shown in Fig. 12(b). Under these conditions the positive ion flux was composed of 0.6% Ar^+, 99% of Cl_2^+ and 0.4% Cl^+. The large percentage of molecular ions was due to charge exchange collisions of Ar^+ and Cl^+ with molecular chlorine, converting the atomic ions to molecular ions. For larger frequencies (approaching and exceeding the ion plasma frequency), most of the applied voltage drops across the bulk plasma and the sheath electric fields are rather small. This results in very low energy ions of almost isotropic angular distribution. As the bias frequency is lowered more of the applied voltage drops across the sheaths and the ion energy increases. Of course, collisions with neutral gas contribute to reduce the ion energy.

5. Conclusions

Ion–ion plasmas can form in the late afterglow of pulsed discharges or downstream of continuous wave discharges in electronegative gases. In ion–ion plasmas, negative ions replace electrons as the negative charge carriers. As a result, the properties of ion–ion plasmas are quite different than those of conventional electron–(positive) ion plasmas. For example, the plasma potential is not the most positive potential in the system, and a negative ion sheath alternates with a positive ion sheath next to a radio frequency biased (RF) electrode. Application of a RF bias to an ion–ion plasma can be beneficial for

microelectronics processing. For a relatively large range of bias frequencies (up to the ion plasma frequency), each electrode is bombarded alternately by energetic positive and negative ions during an RF bias cycle. This alternate bombardment by positive and negative ions may help alleviate charging and notching effects associated with conventional electron-ion plasmas. For bias frequencies greater than the plasma frequency, however, the electrode is bombarded simultaneously by low energy positive and negative ions with ion energies approaching the ion temperature. At low bias frequencies, the peak ion flux in an RF cycle is limited by ion diffusion and is independent of the applied bias potential. The peak ion flux may be increased by lowering the pressure or by using the bias frequency approaching the ion plasma frequency. High bias voltages and low pressures to suppress collisions are necessary to increase the energy of ions bombarding the substrate. Ion–ion plasmas are also of importance in negative ion sources, dusty plasmas, and the D-layer of the earth's atmosphere.

Acknowledgments

Financial support for this work was provided by the National Science Foundation (CTS-0072854 and CTS-0227232), and the State of Texas (Texas Advanced Technology Program).

References

[1] S.M. Rossnagel, J.J. Cuomo, W.D. Westwood (Eds.), Handbook of Plasma Processing Technology, Noyes Publications, Park Ridge, NJ, 1990.
[2] M.A. Leiberman, A.J. Lichtenberg, Principles of Plasma Discharges and Materials Processing, John Wiley and Sons, New York, 1994.
[3] M. Lampe, W.M. Manheimer, R.F. Fernsler, S.P. Slinker, G. Joyce, Plasma Sources Sci. Technol. 13 (2004) 15.
[4] P.G. Daniels, R.N. Franklin, J. Snell, J. Phys. D: Appl. Phys. 23 (1990) 823.
[5] (a) L.D. Tsendin, Zh. Tekh. Fiz. 59 (1989) 21;
(b) L.D. Tsendin, Sov. Phys. Tech. Phys. 34 (1989) 11.
[6] I.G. Kouznetsov, A.J. Lichtenberg, M.A. Lieberman, J. Appl. Phys. 86 (1999) 4142.
[7] V.I. Kolobov, D.J. Economou, Appl. Phys. Lett. 72 (1998) 656.
[8] A. Kono, J. Phys. D: Appl. Phys. 32 (1999) 1357.
[9] J. Matsui, N. Nakano, Z.L. Petrovic, T. Makabe, Appl. Phys. Lett. 78 (2001) 883.
[10] (a) S. Samukawa, T. Mieno, Plasma Sources Sci. Technol. 5 (1996) 132;
(b) S. Samukawa, Appl. Phys. Lett. 68 (1996) 316;
(c) S. Samukawa, H. Ohtake, T. Mieno, J. Vac. Sci. Technol. A 14 (1996) 3049.
[11] T. Shibayama, H. Shindo, Y. Horiike, Plasma Sources Sci. Technol. 5 (1996) 254.
[12] T.H. Ahn, N. Nakamura, H. Sugai, Plasma Sources Sci. Technol. 5 (1996) 139.
[13] V. Midha, D.J. Economou, Plasma Sources Sci. Technol. 9 (2000) 256.
[14] P. Subramonium, M.J. Kushner, J. Vac. Sci. Technol. A 22 (2004) 534.
[15] S. Samukawa, K. Sakamoto, K. Ichiki, J. Vac. Sci. Technol. A 20 (2002) 1566.
[16] F.A. Hass, L.M. Lea, A.J.T. Holmes, J. Phys. D: Appl. Phys. 24 (1991) 1541.
[17] M. Bacal, A. Hatayama, J. Peters, IEEE Trans. Plasma Sci. 33 (2005) 1845.
[18] W. Swider, Ionospheric Modeling, Birkhauser-Verlag, Berlin, 1988.
[19] S. Panda, D.J. Economou, L. Chen, J. Vac. Sci. Technol. A 19 (2001) 398.
[20] A. Hatayama, T. Matsumiya, T. Sakurabayashi, M. Bacal, Rev. Scientific Instrum. 77 (2006) 1.
[21] W. Oohara, R. Hatakeyama, Phys. Rev. Lett. 91 (2003) 205005.
[22] V. Midha, D.J. Economou, J. Appl. Phys. 90 (2001) 1102.
[23] J.S. Newman, Electrochemical Systems, Prentice Hall, 1973.
[24] H. Amemiya, in: H. Kikuchi (Ed.), Dusty and Dirty Plasmas, Noise, and Chaos in Space and in the Laboratory, Plenum Press, 1994.
[25] H. Amemiya, J. Phys. D: Appl. Phys. 23 (1990) 999.
[26] S.A. Gutsev, A.A. Kudryavtsev, V.A. Romanenko, Tech. Phys. 40 (1995) 1131.
[27] A.A. Kudryavtsev, L.D. Tsendin, Tech. Phys. Letts. 26 (2000) 582.
[28] L.J. Overzetr, B.A. Smith, J. Kleber, S.K. Kanakasabapathy, Jpn. J. Appl. Phys. 36 (1997) 2443.
[29] G.A. Hebner, C.B. Fleddermann, J. Appl. Phys. 82 (1997) 2814.
[30] M.V. Malyshev, PhD Dissertation, Princeton University, 1999.
[31] M.V. Malyshev, V.M. Donnelly, Plasma Sources Sci. Technol. 9 (2000) 353.
[32] I.D. Kaganovich, B.N. Ramamurthi, D.J. Economou, Phys. Rev. E 64 (2001) 036402.
[33] D. Smith, A.G. Dean, N.G. Adams, J. Phys. D: Appl. Phys. 7 (1974) 1944.
[34] S.K. Kanakasabapathy, L.J. Overzet, V. Midha, D.J. Economou, Appl. Phys. Lett. 78 (2001) 22.
[35] T. Ohmori, T.K. Goto, T. Kitajima, T. Makabe, Appl. Phys. Lett. 83 (2003) 4637.
[36] T. Yagisawa, T. Makabe, IEEE Trans. Plasma Sci. 31 (2003) 521.
[37] T. Ohmori, T. Goto, T. Makabe, J. Phys. D: Appl. Phys. 37 (2004) 2223.